Biological shot-noise and quantum-limited signal-to-noise ratio in affinity-based biosensors

Arjang Hassibi,[a] Sina Zahedi, Reza Navid, Robert W. Dutton, and Thomas H. Lee
Department of Electrical Engineering, Stanford University, Stanford, California 94305-4070

(Received 23 November 2004; accepted 22 December 2004; published online 11 April 2005)

We study the statistical behavior of affinity-based biosensors. The detection uncertainty and noise in such devices originates primarily from probabilistic molecular-level bindings within the sensing regions, and the stochastic mass-transfer processes within the reaction chamber. In this paper, we model the dynamic behavior of these sensory systems by a Markov process, which enables us to estimate the sensor inherent noise power spectral density (PSD) and response time. We also present the methods by which the Markov parameters are extracted from the reaction kinetic rates, diffusion coefficients, and reaction chamber boundary conditions. Using this model, we explain why Poisson shot noise has been reported in such biosensors and additionally predict a Lorentzian profile for the fluctuation PSD. Furthermore, we demonstrate that affinity-based biosensors have a quantum-limited signal-to-noise ratio (SNR). We also show that the SNR decreases as the dimensions are isomorphically scaled down while the biosensor response speed increases, substantiating a fundamental trade-off between biosensor speed and accuracy. © *2005 American Institute of Physics*. [DOI: 10.1063/1.1861970]

I. INTRODUCTION

In the past decade, molecular biology has moved from being exclusively a research tool in life sciences to having practical applications in the main stream of medicine. This is mainly due to the capabilities of the existing molecular biology detection platforms, which enable researchers to study and analyze biological molecules much more efficiently and if required, in a high-throughput fashion.

Today, there are a variety of different detection platforms in molecular biology.[1] One of the conventional and widely used techniques is affinity-based sensing. A technique which incorporates a biological or biologically derived sensing element either integrated within or intimately associated with the physiochemical transducer.[2] These sensory systems take advantage of the selectivity and specificity (affinity) of biomolecular interactions, such as DNA-DNA hybridization in gene chips[3] or antibody-antigen interactions in immunoassays.[4] Independent of the molecules involved, detection in affinity-based biosensors calls for the following fundamental steps (see Fig. 1): (i) analyte molecules within the reaction chamber collide with the capturing sites (probes), (ii) the two species form a chemical bond, and ultimately (iii) they take part in a measurable transduction process. From a physical point of view, all affinity-based biosensors share the first two steps, whereas the third step may differ among platforms. The transduction processes can be triggered by either the intrinsic characteristics of analyte, such as charge in ion-sensitive detection devices,[5,6] or an extrinsic entity (reporter molecule) physically attached to the analyte, such as fluorescent spectroscopy labels.[7] In general, the fidelity of the biosensor in terms of signal-to-noise ratio (SNR) is a function of the uncertainty (noise) of all of the aforementioned steps. However, the focus of this paper is the stochastic analysis and quantification of the first two steps which as we will demonstrate, is the dominant source of noise in most systems. Little work has been reported on this subject and this study models the *biological* noise of affinity-based biosensors.

Generally speaking, the detectable signal in all conventional sensory systems (including affinity-based biosensors) is generated by the aggregate contribution of individual events (e.g., collision, absorption, emission, etc.), originating from *probabilistic* microscopic systems. In electronic and optoelectronic sensors, for example, the microscopic components of the systems are electrons and photons within solid-state matter. Accordingly, the dynamical behavior of such

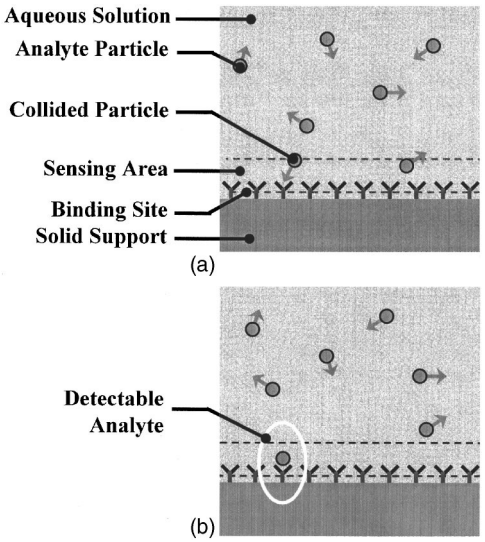

FIG. 1. Detection in affinity-based sensors requires (a) collision of analyte particles with the binding sites followed by (b) analyte capturing and transduction processes.

[a]Electronic mail: arjang@stanford.edu

system, characterized by the expected response and the spontaneous fluctuation (noise), can be characterized by statistical mechanical methods described for electrons and photons.[8,9] In affinity-based biosensors on the other hand, the microscopic components of the system are not small particles like electrons anymore; they are molecules. Since molecules are large-scale quantum-mechanical entities[10] (systems with a large number of discrete states), for the purpose of stochastic analysis, we can still apply similar approaches used for electron devices.[11,12] Quantum chemical and biological systems are essentially more complicated than quantum electronic systems; nevertheless, because of their similarity at the elemental level, we anticipate signal-dependent fluctuations in the form of Poisson shot noise, which is common in many solid-state optoelectronic devices.[9] In this study, we examine this similarity, show its biophysical origin, and comprehensively quantify its behavior in affinity-based biosensors.

It is important to realize that affinity-based biosensors essentially comprise of considerably less number of probabilistic particles compared to optoelectronic sensors. Thus, the mesoscopic signal fluctuation (biological shot noise) quantified in this paper is expected to be observed in much larger dimensions. This observation has been previously reported in DNA microarrays platforms[13] as well as in many other affinity-based transducers.[14–18] In addition, we predict that this type of noise, i.e., biological shot noise, will become significantly more important because of the trend toward implementation of small-scale microfabricated affinity-based biosensors.[19–23] The analytical results of this paper can conceivably aid the sensor designer in better understanding the fundamental trade-offs among scaling, SNR, and response time.

To comprehensively study the SNR of affinity-based biosensors, initially in Sec. II, we introduce the mathematical methods to model the statistical behavior of analyte capturing, considering the binding kinetics and the mass-transfer processes using a Markov model. We will explain how the model can be applied to extract a closed-form noise solution and settling time approximation in Sec. III. Additionally, we derive the quantum-limited SNR (defined as the maximum achievable SNR) of these systems in both the presence and absence of the transducer noise. As a practical numerical example, which verifies the accuracy of the predicted results, we utilize the stochastic model to investigate the behavior of a hybridization-based DNA sensor in Sec. IV. The theoretical prediction for noise calculated in this paper essentially proves the existence of biological shot noise with a Lorentzian power spectral density (PSD).

II. BIOSENSOR STOCHASTIC MODEL

A. Analyte motion

Molecules, cells, and many other analytes immersed in the aqueous reaction chamber of biosensors are subject to thermal fluctuations and, perhaps on particular sensory platforms, subject to electromagnetic or mechanical forces. While mechanical movement (e.g., convection) and electromagnetic forces (e.g., electrophoresis) are in some sense deterministic, thermal fluctuation is random in nature. Thermal

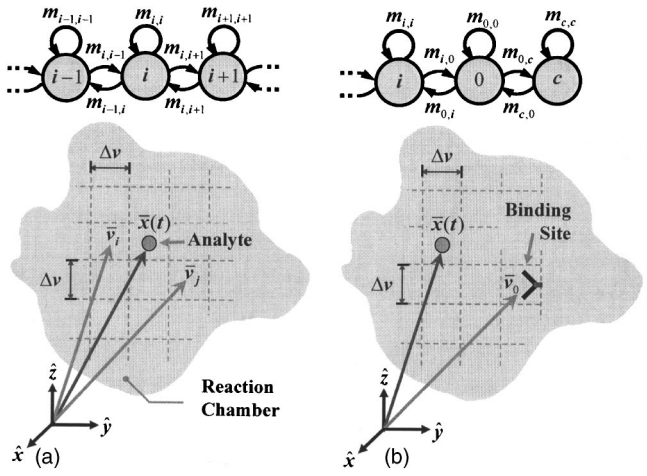

FIG. 2. Markov model for (a) probabilistic motion in the reaction chamber and (b) motion in the presence of immobilized binding sites. Each coordinate corresponds to a state in the process where particles can move into or leave. $\overline{x}(t)$ represents the location of the analyte particle at time t and $\overline{v}_i$ defines the coordinates of the state i in the system.

fluctuations of a particle from a microscopic point of view follow the characteristics of a typical random-walk process[24] (i.e., Brownian motion), which results in a diffusive spreading in macroscopic systems.

It is challenging to statistically follow the motion of each molecule in the general case using continuity equation formulation. However, we can consider a Markov process[25] to model the particle stochastic behavior within the reaction chamber. In this model, each state of the process corresponds to a fixed coordinate within the reaction chamber [Fig. 2(a)]. The transition probabilities are subsequently defined as the probability analyte particles moving from each coordinate (state) to the other in a sufficiently small time interval Δt. The main advantage of this type of modeling is the stochastic nature of the model, which calculates the probability distribution function (pdf) of the analyte particles. Additionally, we can easily derive the expected behavior (ensemble average) of the system, a quantity that is generally calculated using continuity-based equation formulation.

For two arbitrary coordinates $\overline{v_i}$ and $\overline{v_j}$ in the system, represented by states i and j, the state transition probability from state i to j for an analyte particle in time interval Δt is denoted by $m_{i,j}$

$$m_{i,j} = \mathrm{Prob}[\overline{x}(\Delta t) = \overline{v_i} | \overline{x}(0) = \overline{v_j}]. \tag{1}$$

where $\overline{x}(0)$ and $\overline{x}(\Delta t)$ specify the coordinate of an analyte particle at times 0 and Δt, respectively. The particle transition matrix M can be constructed, where its ijth element $m_{i,j}$ is defined in (1) ($M \in R^{N \times N}$ and N is the total number of states). In such a system if the analyte particle has the probability distribution of $\rho(0)$ at time zero across the state space, where $\rho(t) \in R^N$ for all t, at Δt we have

$$\rho(\Delta t) = M\rho(0). \tag{2}$$

Typical biosensor structures have a number of analyte particles within the reaction chamber. Provided that the motion of analyte particles is statistically independent, M and $\rho(t)$ become independent, resulting in a homogeneous Mar-

kov process. Note that this is, in fact, a realistic model for most biosensors since statistical motion in such systems is only governed by the analyte particles interaction with the solution molecules and not by analyte-analyte interaction. In this scenario (a homogeneous Markov process) we can calculate the spatial probability distribution of the analyte particles in all time increments dividable by Δt, given the initial distribution $\rho(0)$, such that

$$\rho(k\Delta t) = M^k \rho(0), \tag{3}$$

where k is an integer number. If we have n particles in the system we can also define a spatial concentration distribution of the particles $C(t)$, where $C(t) = n\rho(t)$. Exact formulations like (3) can be implemented for $C(t)$, except for the transition matrix that might become a function of n, which is defined as M_n. In this general case we have

$$n\rho(k\Delta t) = C(k\Delta t) = M_n^k C(0) = nM_n^k \rho(0). \tag{4}$$

Matrix M (or M_n) can theoretically be estimated for any small time increment Δt, given the exact statistics of the mass transport process described by the continuity equation.[24]

B. Analyte capturing

Now that we have a statistical model of mass relocation within the solution, we need to incorporate the boundary conditions of the reaction chamber. The boundary conditions for conventional biosensors are either purely reflective (inert walls of the chamber and the surface of the solution) or selectively absorbing (surfaces where probes exist). Incorporation of reflective boundaries into the Markov model is carried out by assigning zero probability for particles to move beyond boundaries. However, for selective absorption we need to have a probabilistic model of the collision and interaction process.

Analyte collision with the binding sites results in different possible outcomes (reactive, elastic, and inelastic collisions).[26] As a result, we can introduce a probabilistic model to describe the specific binding of an analyte particle X to a single probe Y in an affinity-based sensor [Fig. 2(b)]. To begin with, we assume that Y is confined (immobilized) within a certain coordinate (e.g., state 0), which is valid for most biosensor structures. Now we can state that any meaningful interaction between X and Y at time t only occurs when $\overline{x}(t) = \overline{v}_0$ (i.e., molecule X is in intimate proximity of Y). If the bulk-phase reaction between X and Y species has the association rate k_1 and disassociation rate of k_{-1}, where (symbol [ ] indicates concentration)

$$\begin{cases} X + Y \overset{k_1, k_{-1}}{\leftrightarrow} XY \\ \dfrac{d[XY]}{dt} = k_1[X][Y] - k_{-1}[XY] \end{cases}, \tag{5}$$

we can apply the following approximation to find the transition probabilities between captured state c of the analyte and the collided state 0:

$$m_{c,0} = k_1[Y_m]\Delta t,$$

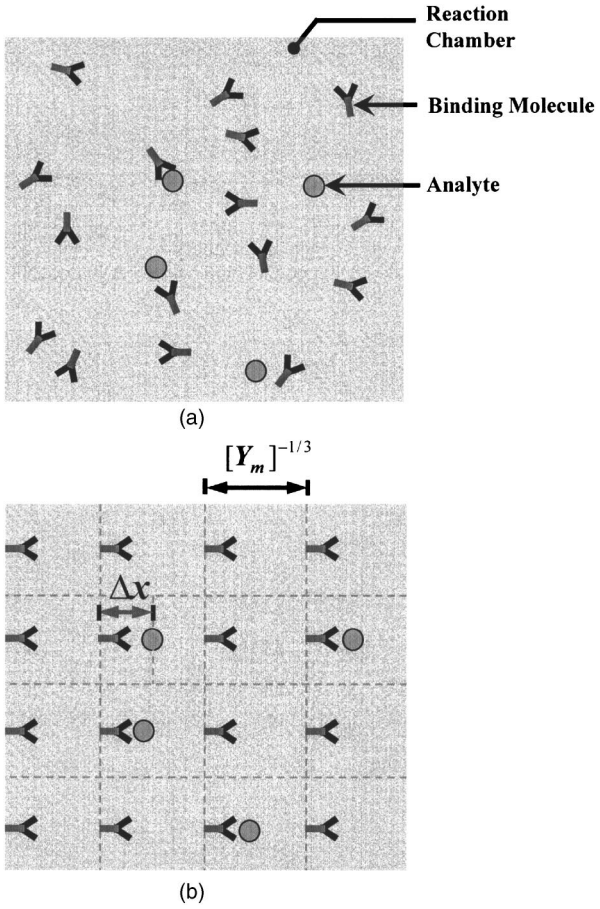

FIG. 3. When the concentration of binding molecules $[Y_m]$ is high enough that the reaction kinetics becomes insensitive to its increase, we practically ensure that (a) every analyte molecule has effectively a Y molecule in its proximity. This is equivalent in average to (b), a system where each Y molecule occupies a volume equal to $[Y_m]^{-1}$, and analyte molecules have a reactive distance of $\Delta x = 1/2[Y_m]^{-1/3}$.

$$m_{0,c} = k_{-1}\Delta t, \tag{6}$$

where $m_{c,0}$ and $m_{0,c}$ are also defined as the association and disassociation probabilities and $[Y_m]$ is the saturation concentration of Y in (5). The physical justification for (6) comes from the fact that in the bulk-phase saturation concentration of Y, we ensure that all X particles are effectively in close proximity of Y molecules [Fig. 3(a)]. In this case individual Y molecules on average occupy a $[Y_m]^{-1}$ volume [Fig. 3(b)] which is equivalent to when $\overline{x}(t) = \overline{v}_0$ in the Markov model if $\Delta x = 1/2[Y_m]^{-1/3}$. Consequently, the reaction rate of X at state 0 should have similar kinetics as when $[Y_m]$ in bulk phase, which results in (6). It is imperative to understand that we can use the macroscopic rates k_1 and k_{-1} to define $m_{c,0}$ and $m_{0,c}$ only when individual molecule binding incidents are statistically independent, Δt is small enough that all entries in M_n are much smaller than one, and Δx is equal to $1/2[Y_m]^{-1/3}$. Using (6) for absorbing boundaries and (4) for the mass relocation and reflection cases, we can statistically analyze the biosensor structure in its entirety (see Fig. 4).

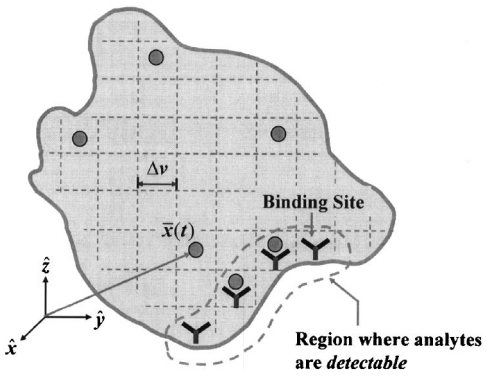

FIG. 4. General Markov model for affinity-based biosensors with N possible states for the analyte particles including captured states.

C. Stochastic analysis

1. System equilibrium distribution

It is important to realize at this point that the transition matrix $\boldsymbol{M_n}$ can be utilized to inspect various characteristics of the system without the need of applying (2) and (3) for numerical simulation. We can easily prove that the general solution $\rho(t)$, which defines the analyte distribution at time t, given initial condition $\rho(0)$, is derived using the following:[27]

$$\rho(t) = \exp([\boldsymbol{M_n} - \boldsymbol{I}]\Delta t^{-1} t)\rho(0) = \boldsymbol{H_n}(t)\rho(0), \tag{7}$$

where $\boldsymbol{I}$ is the unity matrix with the same dimensions as $\boldsymbol{M_n}$. Matrix $\boldsymbol{H_n}(t)$ advances the initial distribution in time and can be calculated using the matrix exponential function, which in effect exponentiates eigenvalues of the matrix. We can demonstrate that the stochastic model for a biosensor system with n analyte particles and no analyte sink or source terms becomes a closed homogeneous Markov process where $\boldsymbol{M_n}$ has a single eigenvalue equal to one. All other eigenvalues of $\boldsymbol{M_n}$ are less than one, ensuring a single equilibrium mode associated with a single equilibrium distribution ρ_E described by the eigenvector of the largest eigenvalue. It can be shown that $\boldsymbol{M_n}$ and $\boldsymbol{H_n}(t)$ share ρ_E such that

$$\rho_E = \boldsymbol{H_n}(t)\rho_E. \tag{8}$$

2. Settling time

The next logical question to ask is how long it will take for the system illustrated in Fig. 4 to reach equilibrium. If the initial analyte concentration is known, using (7) one can easily calculate the time necessary to reach such a state. However, if the initial condition itself is random (usually the case in biosensors) other approaches should be explored. One approach proposed here provides a pessimistic approximation for the settling time and is based on the analysis of all other eigenvalues of $\boldsymbol{M_n}$ which are smaller than one. The upper bound (worst case scenario) for the system settling time can be calculated by the sum of all individual time constants $\tau_1, \tau_2, \ldots, \tau_{N-1}$, associated with the eigenvalues of $\boldsymbol{M_n}$. If $\boldsymbol{M_n} \in \boldsymbol{R}^{N\times N}$ has eigenvalues $\lambda_1, \lambda_2, \ldots, \lambda_{N-1}$, the worst case time constant τ_T can be derived from

$$\tau_T = \sum_{r=1}^{N-1} \tau_r = \sum_{r=1}^{N-1} \frac{\Delta t}{|\lambda_r|}. \tag{9}$$

Note that this approach is similar to the method of open circuit time constants (zero value time constants),[28] which is used to estimate the bandwidth of specific linear circuits.

3. Power spectral density

To quantify the biological noise of the system, we need to characterize the fluctuation of particles in every state, particularly state c, which the affinity sensors observe. To do this at equilibrium, we need to first evaluate all autocorrelation functions of the set of stationary processes described by $\boldsymbol{X_i}(t)$ functions, where $1 \leqslant i \leqslant N$ is any state of the systems and

$$\boldsymbol{X_i}(t) = \begin{cases} 1 & \text{if } \overline{x}(t) = \overline{v_i} \\ 0 & \text{else,} \end{cases} \tag{10}$$

i.e., $\boldsymbol{X_i}(t) = 1$ if there is a particle at state i at time t, and zero otherwise. $\boldsymbol{R_{X_i}}(\tau)$, the autocorrelation of $\boldsymbol{X_i}(t)$, is then defined as

$$\boldsymbol{R_{X_i}}(\tau) = \boldsymbol{E}[\boldsymbol{X_i}(t+\tau)\boldsymbol{X_i}(t)]. \tag{11}$$

The term under the expectation is nonzero only when $\boldsymbol{X_i}(t+\tau)\boldsymbol{X_i}(t) = 1$. Hence $\boldsymbol{R_{X_i}}(\tau) = \text{Prob}[\boldsymbol{X_i}(t+\tau)\boldsymbol{X_i}(t) = 1]$ or

$$\boldsymbol{R_{X_i}}(\tau) = \text{Prob}[\boldsymbol{X_i}(t+\tau) = 1 | \boldsymbol{X_i}(t) = 1]\text{Prob}[\boldsymbol{X_i}(t) = 1]. \tag{12}$$

By using the definition of $\boldsymbol{H_n}(\tau)$ from (7) we have

$$\boldsymbol{R_{X_i}}(\tau) = \boldsymbol{h_{ii}}(|\tau|)\rho_{i,E}, \tag{13}$$

where $\rho_{i,E} = \text{Prob}[\boldsymbol{X_i}(t) = 1]$ is the probability of $\boldsymbol{X}$ being at state i at equilibrium (extracted from ρ_E) and $\boldsymbol{h_{ii}}(\tau)$ is the ith diagonal entry of $\boldsymbol{H_n}(\tau)$. The PSD of this process $\boldsymbol{S_{X_i}}(f)$ is the Fourier transform of (13), where

$$\boldsymbol{S_{X_i}}(f) = \rho_{i,E} \int_{-\infty}^{+\infty} \boldsymbol{h_{ii}}(|\tau|) e^{-j2\pi f} df. \tag{14}$$

If we have n-independent particles we can still use (13) and (14) to find the overall autocorrelation function of the number of particles $\boldsymbol{R_{n_i}}(\tau)$ by

$$\begin{aligned} \boldsymbol{R_{n_i}}(\tau) &= \boldsymbol{E}\left[\sum_{n} \boldsymbol{X_i}(t+\tau) \sum_{n} \boldsymbol{X_i}(t)\right] \\ &= (n^2 - n)\boldsymbol{E}[\boldsymbol{X_i}(t)]^2 + n\boldsymbol{R_{X_i}}(\tau) \\ &= (n^2 - n)(\rho_{i,E})^2 + n\boldsymbol{h_{i,i}}(|\tau|)\rho_{i,E}. \end{aligned} \tag{15}$$

Accordingly the unilateral (single-sided) PSD of the number of particles in state i defined by $\boldsymbol{S_{n_i}}(f)$ is

$$\boldsymbol{S_{n_i}}(f) = 2\pi(n^2 - n)(\rho_{E,i})^2 \delta(f) + 2n\boldsymbol{S_{X_i}}(f). \tag{16}$$

It is evident from (11) that the expected value of n-independent particles in state i, $\boldsymbol{E}[\Sigma_n \boldsymbol{X_i}]$, becomes $n\rho_{i,E}$. To find the variance of the same process $\sigma^2_{n_i}$, we have

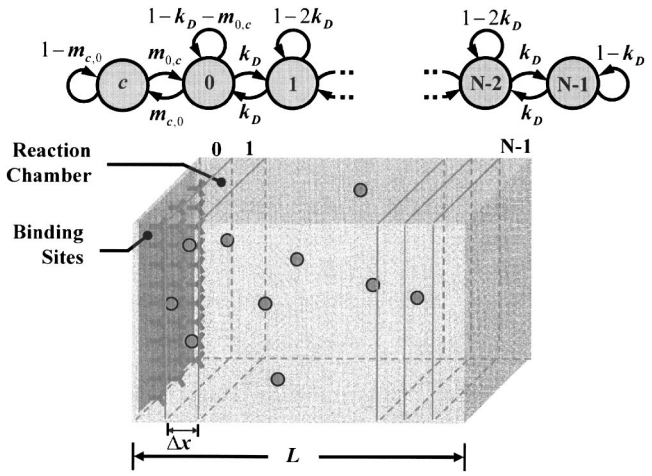

FIG. 5. An affinity biosensors structure with a cubic reaction chamber where mass-transfer processes are only relevant in one dimension.

$$\sigma_{n_i}^2 = E\left[\sum_n X_i(t)\sum_n X_j(t)\right] - \left\{E\left[\sum_n X_i(t)\right]\right\}^2 = n\rho_{i,E}(1-\rho_{i,E}). \quad (17)$$

Note that while (11)–(17) are derived assuming a homogeneous process (no analyte-analyte molecular interactions), the same methodology can still be used for inhomogeneous processes if they have an equilibrium distribution. The only necessary modification is that a transition matrix at equilibrium for the nonhomogeneous process, if any, must be put in the formulations to find the respective $h_{ii}(|\tau|)$ function. This method is essentially a linearization technique. Thus it is valid only when the fluctuations in an existing equilibrium concentration are very small compared to the average concentration (small signal approximation).

III. ONE-DIMENSIONAL BIOSENSOR

A. Transition matrix

As a descriptive example which summarizes the behavior of most biosensors, such as planar arrays and ion-sensitive field-effect transistor (ISFET)-based sensors,[3,21] we now consider a sensor structure with a cubic reaction chamber of dimension L. In this specific system, the probes are only located at one side of the cube. As shown in Fig. 5, the mass relocation processes are relevant in only one dimension. Hence, a one-dimensional Markov process with $N+1$ states ($N=L\Delta x^{-1}$) becomes an applicable model for analyte motion. For very small Δt, the transition matrix M_n becomes very sparse since we can assume that each particle can only move between adjacent states, e.g., i and $i+1$. The value of $m_{i,i+1}$ in the general case can be formulated using the following:

$$m_{i,i+1} = D\Delta t\|\overline{v}_i - \overline{v}_{i+1}\|^{-2} + f_{i,i+1}\Delta t\|\overline{v}_i - \overline{v}_{i+1}\|^{-1}, \quad (18)$$

where D is the analyte diffusion coefficient, $\|\overline{v}_i-\overline{v}_{i+1}\|$ is the distance between states i and $i+1$, and $f_{i,i+1}$ is the effective directional velocity from i to $i+1$ contributed by local drift and convection. In conventional affinity-based sensors the $f_{i,i+1}$ terms are generally designed to be zero since any net drift or convection can possibly bias molecular capturing and reduce specificity. In the presence of solution mixing, convection is indeed present but since the induced mass relocation is deliberately set to be nondirectional and *random* with an average local velocity of zero, we can still consider $f_{i,i+1}=0$. The only modification necessary to the formulation in (18) is an increase in the diffusion coefficient. Subsequently, in this paper we will assume that $m_{i,i+1}$ is location independent and equal to $D\Delta t\|\overline{v}_i-\overline{v}_{i+1}\|^{-2}$.

The transition matrix $M_n \in R^{(N+1)(N+1)}$ with capturing at the surface with kinetics as defined in (5) becomes

$$M_n = \begin{bmatrix} 1-m_{c,0} & m_{0,c} & 0 & & 0 \\ m_{c,0} & 1-m_{0,c}-k_D & k_D & \cdots & 0 \\ 0 & k_D & 1-2k_D & & 0 \\ & \vdots & & \ddots & \vdots \\ & & & & k_D \\ 0 & 0 & 0 & \cdots & 1-k_D \end{bmatrix}, \quad (19)$$

where $m_{c,0}$ and $m_{0,c}$ can be derived using (6), and the value of k_D here can be estimated from (18) which becomes equal to $D\Delta t\Delta x^{-2}$,[24,29] where $\Delta x=1/2[Y_m]^{-1/3}$. In the probability distribution vector of this system $\rho(t)$, the first entry $\rho_c(t)$ is the probability of being in the captured state c and the ones after that [i.e., $\rho_0(t),\rho_1(t),\ldots,\rho_{N-1}(t)$] correspond to the probability of particles being in coordinate zero to $N-1$.

B. Equilibrium distribution

To find the equilibrium probability distribution we should find the eigenvector associated with the eigenvalue of one in (19). By carrying out this procedure we can deduce that the analyte probability distribution in the bulk (states zero to $N-1$) becomes uniform, a result which from a physical point of view is legitimate since diffusion is the only mass transport process in the bulk. If we have n analyte particles in the system at equilibrium, the analyte concentration in state i of the bulk $\rho_{i,E}$ becomes

$$\rho_{i,E} = n\left(\frac{m_{0,c}}{m_{c,0}+Nm_{0,c}}\right) = n\left(\frac{k_{-1}}{k_1[Y_m]+Nk_{-1}}\right). \quad (20)$$

Accordingly the concentration of captured particles becomes

$$\rho_{c,E} = n\left(\frac{m_{c,0}}{m_{c,0}+Nm_{0,c}}\right) = n\left(\frac{k_1[Y_m]}{k_1[Y_m]+Nk_{-1}}\right). \quad (21)$$

C. Settling Time

To find the settling time of the system described by (9), we are required to find the eigenvalues of M_n. It can be shown that the matrix $[I_{(N+1)(N+1)}-M_n]/\Delta t$ has all the eigenvalues of M_n, except for the ones which are equal to one. Now if the describing function of this matrix is defined as $F(s)=\det[sI-M_n]$, then from (19) we have

$$\boldsymbol{F}(\boldsymbol{s}) = \det\begin{bmatrix} \boldsymbol{s}-\boldsymbol{k}_{-1}\Delta\boldsymbol{t} & \boldsymbol{k}_1[\boldsymbol{Y}_m]\Delta\boldsymbol{t} & 0 & & 0 \\ \boldsymbol{k}_{-1}\Delta\boldsymbol{t} & \boldsymbol{s}-(\boldsymbol{k}_1[\boldsymbol{Y}_m]+\boldsymbol{D}\Delta\boldsymbol{x}^{-2})\Delta\boldsymbol{t} & \boldsymbol{D}\Delta\boldsymbol{t}\Delta\boldsymbol{x}^{-2} & \cdots & 0 \\ 0 & \boldsymbol{D}\Delta\boldsymbol{t}\Delta\boldsymbol{x}^{-2} & \boldsymbol{s}-2\boldsymbol{D}\Delta\boldsymbol{t}\Delta\boldsymbol{x}^{-2} & & 0 \\ & \vdots & & \ddots & \vdots \\ & & & & \boldsymbol{D}\Delta\boldsymbol{t}\Delta\boldsymbol{x}^{-2} \\ 0 & 0 & 0 & \cdots & \boldsymbol{s}-\boldsymbol{D}\Delta\boldsymbol{t}\Delta\boldsymbol{x}^{-2} \end{bmatrix},$$

$$= \boldsymbol{s}^{N+1} + \boldsymbol{b}_{N+1}\boldsymbol{s}^N + \boldsymbol{b}_N\boldsymbol{s}^{N-1}\cdots + \boldsymbol{b}_1\boldsymbol{s} + \boldsymbol{b}_0. \tag{22}$$

We know that the sum of the reciprocals of the roots for $\boldsymbol{F}(\boldsymbol{s})$ is equal to $-\boldsymbol{b}_1/\boldsymbol{b}_0$. Since reciprocals of roots $\lambda_1^{-1},\lambda_2^{-1},\ldots,\lambda_{N-1}^{-1}$ are indeed the system time constants described in (9), we have $\tau_T=|\boldsymbol{b}_1/\boldsymbol{b}_0|$. For the one-dimensional system in (19), it is straightforward to show that $|\boldsymbol{b}_1/\boldsymbol{b}_0|$ from (21) is

$$\left|\frac{\boldsymbol{b}_1}{\boldsymbol{b}_0}\right| = \frac{2^N(\boldsymbol{D}\Delta\boldsymbol{x})^{-2N-2}\left\{(\boldsymbol{k}_1[\boldsymbol{Y}_m]+\boldsymbol{D}\Delta\boldsymbol{x}^{-2})+\boldsymbol{k}_{-1}+\frac{1}{2}\boldsymbol{N}\boldsymbol{k}_{-1}(\boldsymbol{k}_1[\boldsymbol{Y}_m]+\boldsymbol{D}\Delta\boldsymbol{x}^{-2})+\boldsymbol{k}_{-1}(\boldsymbol{k}_1[\boldsymbol{Y}_m]+\boldsymbol{D}\Delta\boldsymbol{x}^{-2})\boldsymbol{D}\Delta\boldsymbol{x}^2\right\}}{2^N\boldsymbol{k}_{-1}(\boldsymbol{k}_1[\boldsymbol{Y}_m]+\boldsymbol{D}\Delta\boldsymbol{x}^{-2})(\boldsymbol{D}\Delta\boldsymbol{x})^{-2N-2}},$$

$$= \frac{1}{\boldsymbol{k}_{-1}} + \frac{1}{\boldsymbol{k}_1[\boldsymbol{Y}_m]+\boldsymbol{D}\Delta\boldsymbol{x}^{-2}} + \frac{1}{2}\frac{\boldsymbol{N}}{\boldsymbol{D}\Delta\boldsymbol{x}^{-2}} + \frac{1}{\boldsymbol{D}\Delta\boldsymbol{x}^{-2}},$$

$$= \frac{1}{\boldsymbol{k}_{-1}} + \frac{1}{\boldsymbol{k}_1[\boldsymbol{Y}_m]+\boldsymbol{D}/\Delta\boldsymbol{x}^2} + \frac{\Delta\boldsymbol{x}^2}{\boldsymbol{D}}\left[\frac{\boldsymbol{N}}{2}+1\right]. \tag{23}$$

Note that the values of $\Delta\boldsymbol{x}$ and $\boldsymbol{N}$ in (23) are not arbitrary simulation variables but, in fact, have physical meaning. As illustrated in Fig. 5, $\Delta\boldsymbol{x}$ is implicitly set to be the reactive distance between $\boldsymbol{X}$ and $\boldsymbol{Y}$ for a meaningful interaction estimated from the saturation concentration of $\boldsymbol{Y}$. Accordingly for a given reaction chamber depth $\boldsymbol{L}$, $\boldsymbol{N}$ is equal to $2\boldsymbol{L}[\boldsymbol{Y}_m]^{1/3}$. For most practical situations where dimensions of the reaction chamber are much larger than the reactive distance between $\boldsymbol{X}$ and $\boldsymbol{Y}$ such that $\boldsymbol{N}\gg 1$, hence we have the following approximation for settling time τ_T:

$$\tau_T \approx \frac{1}{\boldsymbol{k}_{-1}} + \frac{1}{\boldsymbol{k}_1[\boldsymbol{Y}_m]+4\boldsymbol{D}[\boldsymbol{Y}_m]^{2/3}} + \frac{\boldsymbol{L}}{4\boldsymbol{D}[\boldsymbol{Y}_m]^{1/3}}. \tag{24}$$

Equation (24) illustrates a few intuitive yet important concepts. (i) The settling time definition in systems with diffusive mass relocation processes (i.e., Brownian motion) relies on the dimensions of the lattice size in the model. (ii) As anticipated from a physical point of view, a higher diffusion coefficient results in faster settling time. (iii) The release of analyte particles represented by $\boldsymbol{k}_{-1}$ is independent of size of the chamber and the diffusion coefficient. (iv) If the size of the chamber becomes extremely small or the diffusion coefficient becomes really large, the settling time reaches a maximum value limited by the reaction kinetics.

D. Power spectral density

To find the power spectral density and the mean and variance of the number of particles captured by such a process we can employ (14) in (16). Yet another method, which is suitable for this example, is to collapse the $\boldsymbol{N}+1$ states into only two significant states of equilibrium, the captured state $\boldsymbol{c}$ and the free state $\boldsymbol{c}'$. The transition probability from (1) for $\boldsymbol{c}$ to $\boldsymbol{c}'$ defined by $\boldsymbol{m}_{\boldsymbol{c},\boldsymbol{c}'}$ is the same as $\boldsymbol{m}_{\boldsymbol{c},0}$ since that is the only possible state the particle can go in the time interval $\Delta\boldsymbol{t}$ from state $\boldsymbol{c}$ which is 0. However, for the reverse process, i.e., going from state $\boldsymbol{c}'$ to $\boldsymbol{c}$, the transition probability $\boldsymbol{m}_{\boldsymbol{c}',\boldsymbol{c}}$ is defined by

$$\begin{aligned}\boldsymbol{m}_{\boldsymbol{c}',\boldsymbol{c}} &= \mathrm{Prob}[\overline{\boldsymbol{x}}(\boldsymbol{t}+\Delta\boldsymbol{t})=\overline{\boldsymbol{v}}_{\boldsymbol{c}}|\overline{\boldsymbol{x}}(\boldsymbol{t})\neq\overline{\boldsymbol{v}}_{\boldsymbol{c}}],\\ &= \mathrm{Prob}[\overline{\boldsymbol{x}}(\boldsymbol{t}+\Delta\boldsymbol{t})=\overline{\boldsymbol{v}}_{\boldsymbol{c}}|\overline{\boldsymbol{x}}(\boldsymbol{t})=\overline{\boldsymbol{v}}_0]\\ &\quad\times\mathrm{Prob}[\overline{\boldsymbol{x}}(\boldsymbol{t})=\overline{\boldsymbol{v}}_0|\overline{\boldsymbol{x}}(\boldsymbol{t})\neq\overline{\boldsymbol{v}}_{\boldsymbol{c}}].\end{aligned} \tag{25}$$

which indicates that the transition occurs only when the particle is in state 0 at time $\boldsymbol{t}$. The term $\boldsymbol{m}_{\boldsymbol{c}',\boldsymbol{c}}$ is derived using $\rho_{0,\boldsymbol{E}}$ and $\rho_{\boldsymbol{c},\boldsymbol{E}}$ from (20) and (21) as

$$\boldsymbol{m}_{\boldsymbol{c}',\boldsymbol{c}} = \boldsymbol{k}_1[\boldsymbol{Y}_m]\Delta\boldsymbol{t}\frac{\rho_{0,\boldsymbol{E}}}{1-\rho_{\boldsymbol{c},\boldsymbol{E}}} = \hat{\boldsymbol{k}}_1\Delta\boldsymbol{t}. \tag{26}$$

where $\hat{\boldsymbol{k}}_1$ is the effective association rate. Hence, the new transition matrix for the collapsed system $\boldsymbol{M}'$ becomes

$$\boldsymbol{M}' = \begin{bmatrix} 1-\boldsymbol{k}_{-1}\Delta\boldsymbol{t} & \hat{\boldsymbol{k}}_1\Delta\boldsymbol{t} \\ \boldsymbol{k}_{-1}\Delta\boldsymbol{t} & 1-\hat{\boldsymbol{k}}_1\Delta\boldsymbol{t} \end{bmatrix}. \tag{27}$$

Accordingly

TABLE I. The closed-form approximations for the statistical characteristics of a one-dimensional biosensor structure.

Biosensor specification	Closed-form approximation
Settling time constant	$\frac{1}{\boldsymbol{k}_{-1}}+\frac{1}{\boldsymbol{k}_1[\boldsymbol{Y}_m]+4\boldsymbol{D}[\boldsymbol{Y}_m]^{2/3}}+\frac{L}{\boldsymbol{4D}[\boldsymbol{Y}_m]^{1/3}}$
Expected number of analyte particles captured by the binding sites	$\boldsymbol{n}\rho_{\boldsymbol{c},\boldsymbol{E}}=\boldsymbol{n}\left(\frac{\boldsymbol{k}_1[\boldsymbol{Y}_m]}{\boldsymbol{k}_1[\boldsymbol{Y}_m]+\boldsymbol{N}\boldsymbol{k}_{-1}}\right)$
Power spectral density of captured particles	$2\pi(\boldsymbol{n}\rho_{\boldsymbol{c},\boldsymbol{E}})^2\delta(\boldsymbol{f})+\frac{4\boldsymbol{n}\rho_{\boldsymbol{c},\boldsymbol{E}}(1-\rho_{\boldsymbol{c},\boldsymbol{E}})}{(\hat{\boldsymbol{k}}_1+\boldsymbol{k}_{-1})[1+(2\pi\boldsymbol{f})^2/(\hat{\boldsymbol{k}}_1+\boldsymbol{k}_{-1})^2]}$
Quantum-limited SNR	$\boldsymbol{n}\frac{\rho_{\boldsymbol{c},\boldsymbol{E}}}{1-\rho_{\boldsymbol{c},\boldsymbol{E}}}$
SNR in presence of unspecific binding and transducer noise	$\frac{(\boldsymbol{n}\rho_{\boldsymbol{c},\boldsymbol{E}})^2}{\boldsymbol{n}\rho_{\boldsymbol{c},\boldsymbol{E}}(1-\rho_{\boldsymbol{c},\boldsymbol{E}})+\tilde{\boldsymbol{n}}\tilde{\rho}_{\boldsymbol{c},\boldsymbol{E}}(1-\tilde{\rho}_{\boldsymbol{c},\boldsymbol{E}})+\sigma_{\boldsymbol{T}}^2}$
SNR with $\boldsymbol{K}$-independent measurements	$\frac{\boldsymbol{K}(\boldsymbol{n}\rho_{\boldsymbol{c},\boldsymbol{E}})^2}{\boldsymbol{n}\rho_{\boldsymbol{c},\boldsymbol{E}}(1-\rho_{\boldsymbol{c},\boldsymbol{E}})+\tilde{\boldsymbol{n}}\tilde{\rho}_{\boldsymbol{c},\boldsymbol{E}}(1-\tilde{\rho}_{\boldsymbol{c},\boldsymbol{E}})+\sigma_{\boldsymbol{T}}^2}$

$$\boldsymbol{H}'(\tau)=\frac{1}{\hat{\boldsymbol{k}}_1+\boldsymbol{k}_{-1}}\begin{bmatrix}\boldsymbol{k}_{-1}+\hat{\boldsymbol{k}}_1\boldsymbol{e}^{-(\hat{\boldsymbol{k}}_1+\boldsymbol{k}_{-1})\tau} & \boldsymbol{k}_{-1}-\boldsymbol{k}_{-1}\boldsymbol{e}^{-(\hat{\boldsymbol{k}}_1+\boldsymbol{k}_{-1})\tau}\\ \hat{\boldsymbol{k}}_1-\hat{\boldsymbol{k}}_1\boldsymbol{e}^{-(\hat{\boldsymbol{k}}_1+\boldsymbol{k}_{-1})\tau} & \hat{\boldsymbol{k}}_1+\boldsymbol{k}_{-1}\boldsymbol{e}^{-(\hat{\boldsymbol{k}}_1+\boldsymbol{k}_{-1})\tau}\end{bmatrix}, \tag{28}$$

and therefore $\boldsymbol{R}_{\boldsymbol{n}_c}(\tau)$, the autocorrelation function of the number of the captured particles by utilizing (15) and (28) becomes

$$\boldsymbol{R}_{\boldsymbol{n}_c}(\tau)=(\boldsymbol{n}^2-\boldsymbol{n})(\rho_{\boldsymbol{c},\boldsymbol{E}})^2+\frac{\boldsymbol{n}\rho_{\boldsymbol{c},\boldsymbol{E}}\boldsymbol{k}_{-1}}{\hat{\boldsymbol{k}}_1+\boldsymbol{k}_{-1}}+\frac{\boldsymbol{n}\rho_{\boldsymbol{c},\boldsymbol{E}}\hat{\boldsymbol{k}}_1}{\hat{\boldsymbol{k}}_1+\boldsymbol{k}_{-1}}\boldsymbol{e}^{-(\hat{\boldsymbol{k}}_1+\boldsymbol{k}_{-1})|\tau|}. \tag{29}$$

We know that when $\tau\to\infty$, in (28)$\boldsymbol{h}_{11}(\infty)\to\rho_{\boldsymbol{c},\boldsymbol{E}}$. Since $\boldsymbol{h}_{11}(\infty)=\boldsymbol{k}_{-1}/(\hat{\boldsymbol{k}}_1+\boldsymbol{k}_{-1})$, we can conclude that $\rho_{\boldsymbol{c},\boldsymbol{E}}=\boldsymbol{k}_{-1}/(\hat{\boldsymbol{k}}_1+\boldsymbol{k}_{-1})$. Hence (29) can be rewritten as

$$\boldsymbol{R}_{\boldsymbol{n}_c}(\tau)=(\boldsymbol{n}\rho_{\boldsymbol{c},\boldsymbol{E}})^2+\boldsymbol{n}\rho_{\boldsymbol{c},\boldsymbol{E}}(1-\rho_{\boldsymbol{c},\boldsymbol{E}})\boldsymbol{e}^{-(\hat{\boldsymbol{k}}_1+\boldsymbol{k}_{-1})|\tau|}. \tag{30}$$

Subsequently, by using (29), the single-sided PSD defined in (16) becomes

$$\boldsymbol{S}_{\boldsymbol{n}_c}(\boldsymbol{f})=2\pi(\boldsymbol{n}\rho_{\boldsymbol{c},\boldsymbol{E}})^2\delta(\boldsymbol{f})+\frac{4\boldsymbol{n}\rho_{\boldsymbol{c},\boldsymbol{E}}(1-\rho_{\boldsymbol{c},\boldsymbol{E}})}{(\hat{\boldsymbol{k}}_1+\boldsymbol{k}_{-1})[1+(2\pi\boldsymbol{f})^2/(\hat{\boldsymbol{k}}_1+\boldsymbol{k}_{-1})^2]}, \tag{31}$$

which demonstrates a Lorentzian (single-pole) profile for the PSD of the number of captured particles. The 3dB bandwidth of the inherent noise PSD in this system represented by $\boldsymbol{f}_{3\mathrm{dB}}$ is accordingly located at $(\hat{\boldsymbol{k}}_1+\boldsymbol{k}_{-1})/2\pi$.

E. Signal-to-noise ratio

To find the signal-to-noise performance of such a system in equilibrium, we should firstly identify the signal as well as noise sources. If the biosensor system is designed to measure the analyte concentration in a reaction chamber and the transduction process only observes captured particles, we can define the signal to be the number of particles in state $\boldsymbol{c}$. The measurement noise in the absence of any transduction noise (detector noise) is then merely generated from the fluctuations of the number of analyte particles in state $\boldsymbol{c}$. In this case the SNR is defined as the signal power divided by the noise power. The signal power is $(\boldsymbol{n}\rho_{\boldsymbol{c},\boldsymbol{E}})^2$ and noise power is expressed in (17). Hence

$$\mathrm{SNR}_{\mathrm{QL}}=\frac{(\boldsymbol{n}\rho_{\boldsymbol{c},\boldsymbol{E}})^2}{\boldsymbol{n}\rho_{\boldsymbol{c},\boldsymbol{E}}(1-\rho_{\boldsymbol{c},\boldsymbol{E}})}=\boldsymbol{n}\frac{\rho_{\boldsymbol{c},\boldsymbol{E}}}{1-\rho_{\boldsymbol{c},\boldsymbol{E}}}. \tag{32}$$

Equation (32) denotes the maximum possible SNR in the absence of any transduction noise and is generally referred to as the quantum-limited SNR, represented by $\mathrm{SNR}_{\mathrm{QL}}$. When the transducer is noisy (generally always the case), the overall SNR should also take into account the added noise of the transducer. If this excess noise is independent of the mass relocation and capturing processes and has the variance of $\sigma_{\boldsymbol{T}}^2$ referred to the number of the captured particles, we have

$$\mathrm{SNR}=\frac{(\boldsymbol{n}\rho_{\boldsymbol{c},\boldsymbol{E}})^2}{\boldsymbol{n}\rho_{\boldsymbol{c},\boldsymbol{E}}(1-\rho_{\boldsymbol{c},\boldsymbol{E}})+\sigma_{\boldsymbol{T}}^2}. \tag{33}$$

In most practical cases for biosensors, analytes are not the only particles which can be captured by the probes. For instance, in hybridization-based DNA detection systems, beside the target DNA fragment, other sequences of DNA in the solution might also bind to the probe with less probability than of the target. This problem is a consequence of imperfect binding sites and generally referred to as the detection specificity. For an ideal biosensor platform in which the sensing area has infinite capacity for particle capturing (no saturation), we are able to calibrate the amount of unspecific capturing by simply subtracting the expected number of unspecific particles from the signal. Nevertheless, the noise caused by these probabilistic yet unspecific particles still exists. If $\tilde{\boldsymbol{n}}$ background particles exist in the system, where each can bind to the sensor surface with probability of $\tilde{\rho}_{\boldsymbol{c},\boldsymbol{E}}$, the new SNR expression becomes

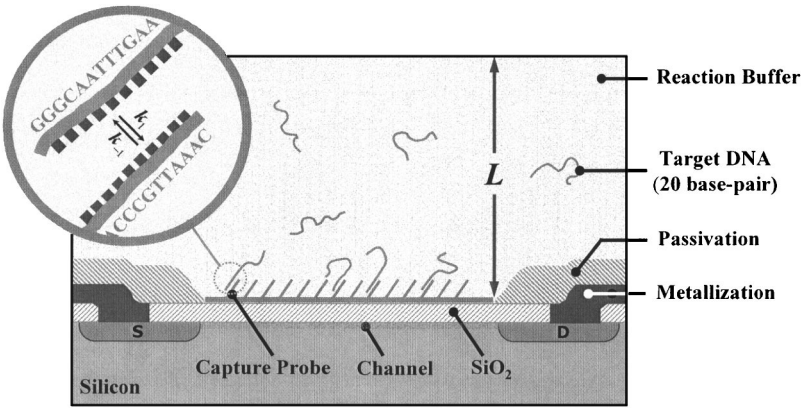

FIG. 6. An electronic DNA hybridization sensor where the ISFET device detects the binding incidents. When charged DNA strands bind to their complementary structures (i.e., binding sites) of the sensing area, the charge profile in the channel is modified. Subsequently, the induced change in channel transconductance is electronically quantified and associated with DNA binding.

$$\mathrm{SNR} = \frac{(\boldsymbol{n}\rho_{c,E})^2}{\boldsymbol{n}\rho_{c,E}(1-\rho_{c,E}) + \tilde{\boldsymbol{n}}\tilde{\rho}_{c,E}(1-\tilde{\rho}_{c,E}) + \sigma_T^2}, \tag{34}$$

given that background particles can take part in transduction process exactly the same way as the analyte particles.

The SNR values in (32)–(34) are for single observations, but in some biosensor platforms multiple samples in time can be acquired (equivalent to low-pass filtering for continuous signals). If these samples are independent (e.g., many $1/\boldsymbol{f}_{-3\mathrm{dB}}$ time samples apart), then for $\boldsymbol{K}$ samples SNR is increased by a factor of $\boldsymbol{K}$. In Table I, we have summarized the closed-form results derived in this section, which predicts the stochastic behavior of one-dimensional affinity-based biosensors.

IV. NUMERICAL EXAMPLE

As a practical example, we analyze the stochastic characteristics of an ISFET device for electronic detection of DNA hybridization.[14] The structure of this specific biosensor consists of a planar field-effect sensing element at the bottom of the reaction chamber with depth of $\boldsymbol{L}$ (see Fig. 6). The detection occurs when the charged analytes (DNA in this case) are captured by the probes which have complementary sequences. Since the analyte is intrinsically a charged particle, binding can create a surface potential change which alters the double layer capacitance of the interface. Capacitance changes in the gate of the FET device change the charge profile of the channel, modulating the drain-source current, which results in detectable electronic output signals.

In this electronic biosensor platform, diffusion is basically the only mass transport process of the analyte in the solution since externally induced drift processes reduce the specificity of the hybridization. The diffusion coefficient of the target molecule (analyte), a single strand 20 base-pair DNA in this example, defined by $\boldsymbol{D_t}$ is estimated to be 1.5×10^{-6} cm^2/s, and $[\boldsymbol{X}]$, the nominal concentration of the DNA, is set to be 0.1 nM ($\approx 6\times10^{10}$ molecules/cm^3), a detectable concentration in fluorescence-based microarray platforms. The approximate binding kinetic rates as well as the simulation specifications are mentioned in Table II. Note that the time increment ($\Delta\boldsymbol{t}=4.7$ μs) is set to its maximum allowable value such that $\boldsymbol{k_D}=1/2$.

The first step in analyzing this biosensor is to create the transition matrix described by (19), assuming that $\boldsymbol{L}=6$ μm (101 states in the Markov model including captured state). Equation (21) suggests that only 2.93% of the DNA molecules in average will bind to the surface at equilibrium. The settling time from (24) is always less than 0.2 s. In Fig. 7, we plotted the result of a Monte Carlo random-walk simulation of 1000 particles in the system for the duration of 0.6 s along with the predictions from (21) and (24). The settling time approximation calculated from (24) sets upper and lower bounds for the quantity of captured analytes. One bound assumes that all 1000 DNA molecules are captured initially,

TABLE II. Specifications of ISFET biosensor for electronic detection of DNA hybridization.

Parameter	Simulation value
DNA diffusion coefficient ($\boldsymbol{D_t}$)	1.5×10^{-6} cm^2/s
DNA concentration ($[\boldsymbol{X}]$)	0.1 nm
Forward binding rate ($\boldsymbol{k_1}$)	3×10^7 M^{-1} s^{-1}
Reverse rate ($\boldsymbol{k_{-1}}$)	5 s^{-1}
Probe saturation concentration ($[\boldsymbol{Y_m}]$)	1 μm
Transduction noise Power (σ_T^2)	1 molecule^2
Simulation lattice size ($\Delta\boldsymbol{x}$)	60 nm
Simulation time increment ($\Delta\boldsymbol{t}$)	4.7 μs

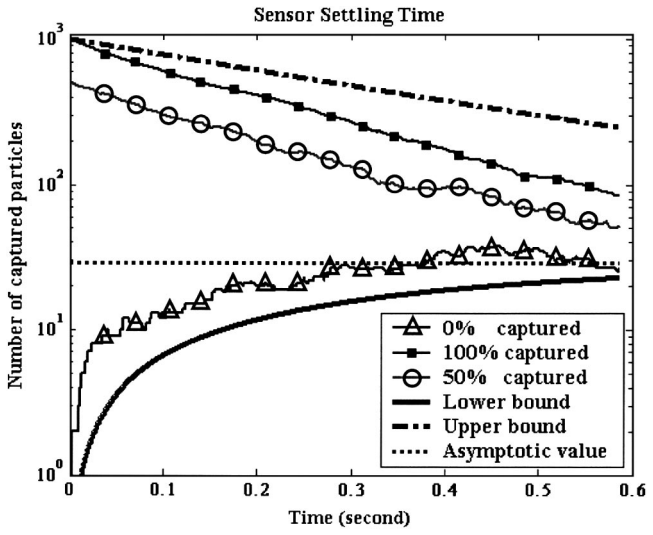

FIG. 7. Transient simulation results of the DNA biosensor where analyte number is 1000. A Monte Carlo random-walk simulation is carried out with three initial distributions. The lower and upper bounds are calculated using (24), and the asymptotic value is derived from (21).

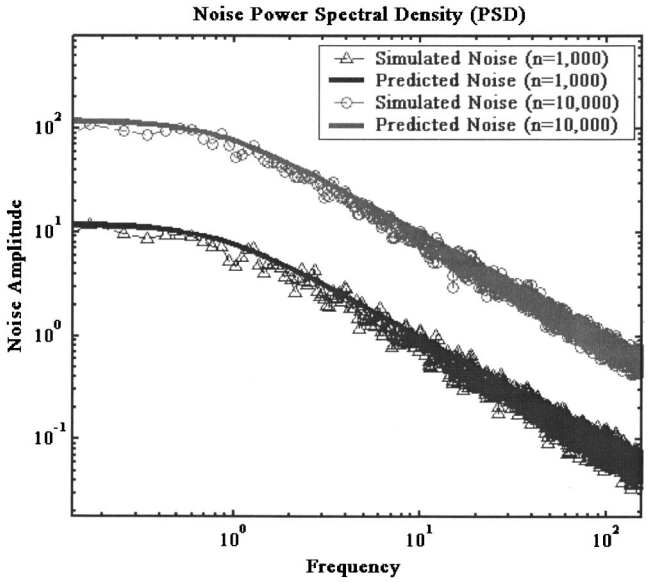

FIG. 8. Simulated PSD of noise for $n=1000$ and $n=10\,000$, which demonstrates the accuracy of the PSD approximation derived in (31).

whereas the other assumes that all reside in the bulk solution with a uniform distribution. The responses within these boundaries correspond to Monte Carlo simulation results given different initial conditions (0%, 50%, and 100% captured initially). The results show the applicability of closed-form solutions, since the transient result all converge faster than the settling time bounds toward an asymptotic value, which suggest 29.3 molecules are in average captured at equilibrium.

Next we look at the fluctuation of the number of captured particles (biological noise) at equilibrium. From (31) we predict a Lorentzian noise PSD with an amplitude proportional to the number of particles in the solution. In Fig. 8 we have plotted the predicted PSD as well as the simulated results for $\boldsymbol{n}=1000$ and $n=10\,000$. Again, the predicted PSD clearly matches Monte Carlo simulations verifying (31).

In Fig. 9, we illustrate the theoretical SNR computed using (33) versus the settling time approximation given in (24), assuming that the system is isomorphically scaled down, i.e., the reaction chamber in all dimensions is scaled. The analyte concentration in this example is kept constant to 0.1 nM. This graph indicates that smaller sensors have faster settling time and reach equilibrium more quickly. However, the SNR of such systems decreases, which suggests a fundamental trade-off between SNR and speed of affinity-based biosensors. This can in turn impose a basic limitation on the size of the sensors for practical applications. Note that for dimensions less than 6 μm in this example, the SNR becomes extremely low, given that the number of analyte particles in the chamber turns out to be very small. This is, in fact, known to be a limitation in many microfluidic analytical systems.[30]

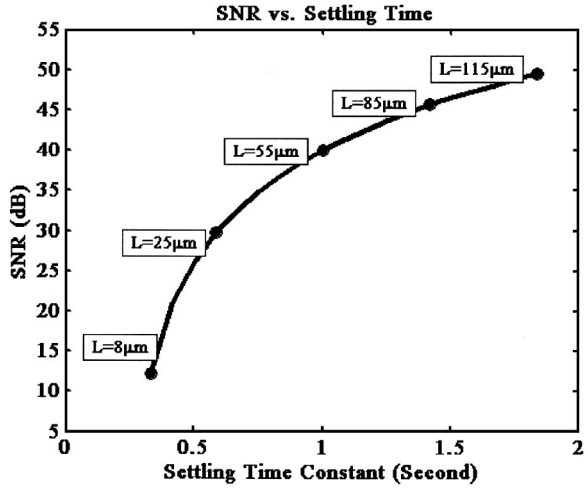

FIG. 9. SNR from (33) vs speed from (23) is plotted as the reaction chamber is isomorphically scaled down, which demonstrates the fundamental trade-off between size and response time of affinity-based biosensors.

V. CONCLUSION

The signal observed in an affinity-based biosensors is a function of captured analyte particles by the corresponding recognition sites and the selective probes. The probabilistic motion and interaction of particles results in a random signal fluctuation (biological noise), which is observed along with transducer noise. We have shown that the random component of signal has a Lorentzian power spectral density and its amplitude is proportional to the concentration of captured particles. The observed signal-to-noise ratio (SNR) of these systems also decreases as the system is isomorphically scaled down, while the system's speed increases. Additionally, we have analytically calculated the general SNR of such sensors and derived the quantum-limited SNR, which denotes an unavoidable uncertainty for each measurement. The methods presented in this paper can be applied to the design of various sensory systems, specifically low-noise biochemical detectors with micro- and nanoscaled transducers. Based on these models, one can also derive a variety of estimation techniques to better detect analytes in biosensors.

ACKNOWLEDGMENTS

This research was partially supported by NSF in support of the Network for Computational Nanotechnology (NCN) and Stanford Network Research Center (SNRC). The authors also want to thank Sam Kavusi, Hossein Kakavand, and Rostam Dinyari for their technical feedback.

[1]E. A. H. Hall, *Biosensors* (Prentice-Hall, Englewood Cliffs, NJ, 1991).
[2]G. T. A. Kovacs, *Micromachined Transducers* (McGraw-Hill, New York, 1998), Chap. 8, p. 722.
[3]M. Schena, *Microarray Analysis* (Wiley, New York, 2003).
[4]E. P. Diamandis and T. K. Christopoulos, *Immunoassays*, 1st ed. (Academic, San Diego, 1996).
[5]P. Bergveld, IEEE Trans. Biomed. Eng. **17**, 70 (1970).
[6]P. Bergveld, Sens. Actuators B **4**, 125 (1991).
[7]J. R. Lacowicz, *Principles of Fluorescence Spectroscopy*, 2nd ed. (Plenum, New York, 1999).
[8]H. A. Hauss, *Electromagnetic Noise and Quantum Optical Measurements* (Springer, New York, 2000), Chap. 4, p. 127.
[9]A. Van der Ziel, *Noise in Solid State Devices and Circuits*, 9th ed. (Wiley, New York, 1986).
[10]I. N. Levine, *Quantum Chemistry*, 5th ed. (Prentice-Hall, New York, 1999), Chap. 16, p. 626.
[11]N. G. Van Kampen, *Stochastic Processes in Physics and Chemistry* (North-Holland, Amsterdam, 1981).

[12]J. I. Steinfield, J. S. Fransisco, and W. L. Hase, *Chemical Kinetics and Dynamics*, 2nd ed. (Prentice-Hall, New York, 1998), Vol. 1, Chap. 10, p. 287.
[13]Y. Tu, G. Stolovitzky, and U. Klein, Proc. Natl. Acad. Sci. U.S.A. **99**, 14031 (2002).
[14]J. Hubble, Biotechnol. Lett. **22**, 1483 (2000).
[15]C. A. Savran, T. P. Burg, J. Fritz, and S. R. Manalis, Appl. Phys. Lett. **83**, 1659 (2003).
[16]J. Min and A. J. Baeumner, Electroanalysis **16**, 724 (2004).
[17]A. Hassibi, T. H. Lee, R. Navid, R. W. Dutton, and S. Zahedi, IEEE 26th International Conference of Engineering in Medicine and Biology, San Francisco, 2004 (unpublished).
[18]S. Zahedi, R. Navid, and A. Hassibi, IEEE 26th International Conference of Engineering in Medicine and Biology, San Francisco, 2004 (unpublished).
[19]R. Thewes *et al.*, Proceedings of the International Solid-State Circuits Conference (ISSCC), San Francisco, 2002 (unpublished), p. 350.
[20]Y. Cui, Q. Wei, H. Park, and C. Lieber, Science **293**, 1290 (2001).
[21]J. Fritz, E. Cooper, S. Gaudet, P. K. Sorger, and S. Manalis, Proc. Natl. Acad. Sci. U.S.A. **99**, 14142 (2002).
[22]R. Hintsche, M. Paeschke, U. Wollenberger, U. Schnakenberg, B. Wagner, and T. Lisec, Biosens. Bioelectron. **9**, 697 (1994).
[23]J. Wang, Anal. Biochem. **71**, 328R (1999).
[24]H. C. Berg, *Random Walks in Biology* (Princeton University Press, New Jersey, 1993).
[25]L. C. Rogers and D. Williams, *Diffusions, Markov Processes, and Martingales*, 2nd ed. (Cambridge University Press, Cambridge, 2000), Vol. 1, Chap. 1.
[26]R. S. Berry, S. A. Rice, and J. Ross, *Physical Chemistry*, 2nd ed. (Oxford University Press, New York, 2000), Chaps. 27–28.
[27]C. T. Chen, *Linear System Theory and Design* (Oxford University Press, New York, 1999), Chap. 4, p. 86.
[28]T. H. Lee, *The Design of CMOS Radio-Frequency Integrated Circuits*, 2nd ed. (Cambridge University Press, Cambridge, 2004), Chap. 8, p. 234.
[29]J. D. Plummer, M. D. Deal, and P. B. Griffin, *Silicon VLSI Technology: Fundamental, Practice and Modeling* (Prentice-Hall, New York, 2000), Chap. 7, pp. 403–405.
[30]M. J. Madou and R. Cubicciotti, Proc. IEEE **91**, 830 (2003).